

## Instabilities and chaos in a multimode, standing-wave, cw dye laser

I. McMackin, C. Radzewicz,\* M. Beck, and M. G. Raymer

*The Institute of Optics, University of Rochester, Rochester, New York 14627*

(Received 28 September 1987; revised manuscript received 23 December 1987)

Experimental and theoretical investigations of a multimode, standing-wave, cw dye laser have been carried out. The optical spectrum of the dye laser was found to evolve by discrete transitions with increasing pump power, between spectra composed of three stable modes and spectra composed of many modes whose amplitudes fluctuate strongly. The variation of the intensities versus time of individual modes of the multimode laser was measured. For pump powers where the spectrum consisted of modes with strongly fluctuating amplitudes, we found that the intensities of individual modes have a correlation time that decreases, and a variance that increases, with increasing pump power. In addition, the fluctuations were found to be deterministically chaotic. This rules out quantum noise as the origin of the fluctuations, a mechanism that had been assumed in many previous studies. We also have carried out numerical simulations of this laser, using a semiclassical model based on third-order, coupled-mode laser theory, which includes population oscillations, four-wave mixing in the gain medium, spatial hole burning, and spontaneous-emission noise. The behavior of the optical spectrum and the fluctuations of single-mode intensities are well modeled for low pump powers. The modeling indicates that four-wave mixing and spatial hole burning are responsible for the discrete transitions in the optical spectrum, and that four-wave mixing drives the strong fluctuations of the individual mode intensities.

### I. INTRODUCTION

An understanding of the dynamics of a broadband, standing-wave, cw dye laser is of intrinsic physical interest in addition to having important practical applications. The central questions to be addressed are: Why does this homogeneously broadened laser oscillate with such a broad optical spectrum (depending on cavity configuration up to 10 000 longitudinal modes can appear in the time-averaged spectrum), and why do the intensities of the individual modes undergo full-scale fluctuations on time scales much longer than the cavity decay time?

Many attempts to understand this behavior have been made.<sup>1-17</sup> A practical motivation is the desirability of developing a quantitative understanding of a laser which is commonly used in intracavity laser spectroscopy (ILS), which is performed by placing a weak absorber inside the laser cavity and observing the resulting absorption dip in the laser emission spectrum.<sup>18,19</sup> Multimode, homogeneously broadened lasers, with a spectral bandwidth that is much broader than the absorption linewidth, have been found to be extremely sensitive when used in ILS, with sensitivities of the order of  $10^{-9}$  cm<sup>-1</sup>.<sup>2</sup> This high sensitivity arises from the homogeneous broadening combined with the existence of many possible modes in which lasing can occur. The laser acts to maintain its total output power at a constant value, while a small loss in one mode can easily cause it to be quenched, with other modes undergoing slight increases in power. An intrinsic limitation to ILS sensitivity appears to be the finite time during which a given mode will lase and thus be able to interact continuously with the absorber.<sup>2,20</sup> This mode "lifetime" or, more properly, correlation time will be denoted  $\tau_c$ . A

simple model of ILS then says that the effective interaction length is  $c\tau_c$ , or the distance light travels in a correlation time. This distance can be in the range  $3 \times 10^3 - 3 \times 10^6$  m, thus making plausible the extreme sensitivity of ILS. One must, therefore, understand the origin of the mode intensity fluctuations in order to understand better the underlying physics of ILS.

Attempts have been made to describe theoretically the origin of the mode intensity fluctuations as arising from quantum noise, i.e., spontaneous emission from the lasing medium.<sup>3,5,7</sup> Indeed, in two-mode ring lasers very near threshold, spontaneous emission is well established to be a source of mode switching instabilities.<sup>21</sup> A rigorous treatment of this type for multimode lasers was carried out by Hioe, who was able to solve analytically for the mode intensity probability distribution and the mode intensity correlation time, using third-order laser theory in the free-running approximation, in which all four-wave mixing terms are neglected.<sup>3</sup> Other models have been based on photon rate equations including stochastic noise terms.<sup>5,7</sup> All of these models result in large mode intensity fluctuations, seeming to lend them some credence. The theory of Kovalenko<sup>7</sup> predicts an increasing mode intensity correlation time with increasing pump power. However, all experiments to date show decreasing correlation time with increasing power.<sup>13,17</sup> In a recent paper by Alvazyan *et al.*, this problem with the model of Kovalenko was partially overcome by including in the stochastic photon rate equations a nonlinear coupling between modes by the effect of stimulated Brillouin scattering.<sup>17</sup>

Nevertheless, all of these previous models neglect four-wave mixing among the modes. Such parametric interactions arise naturally in a semiclassical treatment of the laser, which properly accounts for the coherent dy-

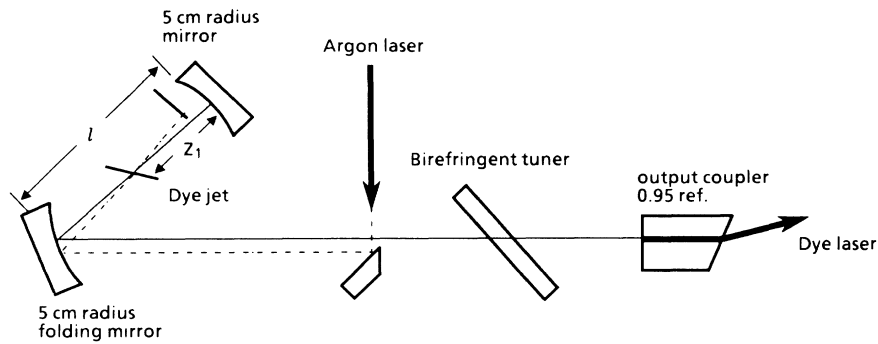


FIG. 1. Schematic diagram of dye-laser cavity (not to scale).

namics of the modes of the electric field.<sup>22,23</sup> We find in the present work that for multimode dye lasers four-wave mixing is the dominant contribution to the fluctuation dynamics.

There exists a large body of theoretical work concerned with the instabilities of homogeneously broadened, multimode lasers.<sup>12,24–28</sup> The work of Brunner *et al.*<sup>12</sup> is the most relevant to our investigations. They found that the mode amplitudes of a homogeneously broadened, multimode laser did not fluctuate, but that the mode amplitudes of an inhomogeneously broadened laser could exhibit time-dependent fluctuations. They studied gas lasers whose gain medium effectively fills the cavity and thus eliminates the influence of spatial hole burning. Spatial hole burning will be discussed in greater detail in Sec. III. It cannot be neglected when modeling the behavior of a laser with a thin gain medium, such as in the present study. Also, Brunner *et al.*<sup>12</sup> neglected the effects of quantum noise in their model, which may not be valid in view of work cited

above. We have included in our model the effects of spatial hole burning and quantum noise.

In this paper we report the results of an experimental and theoretical investigation that addresses several key questions about the behavior of a broadband, standing-wave, cw dye laser.<sup>29</sup> The dye laser studied, shown in Fig. 1, was composed of a three-mirror folded cavity, a single-plate birefringent tuner, and a dye jet formed by a sapphire nozzle. The dye laser was pumped by an intensity-stabilized argon-ion laser. A primary concern is how the optical spectrum varies with pump power. We observed a series of instabilities consisting of abrupt changes in the spectrum as the pump power was varied. Discrete transitions occurred from spectra composed of three stable modes to spectra composed of many modes whose amplitudes fluctuate strongly. In Fig. 2(a) a scanning Fabry-Pérot-interferometer spectrum shows at low pump power three stable modes separated by 2 GHz. The cavity mode spacing was about 300 MHz. When the pump power is increased the frequency separation sud-

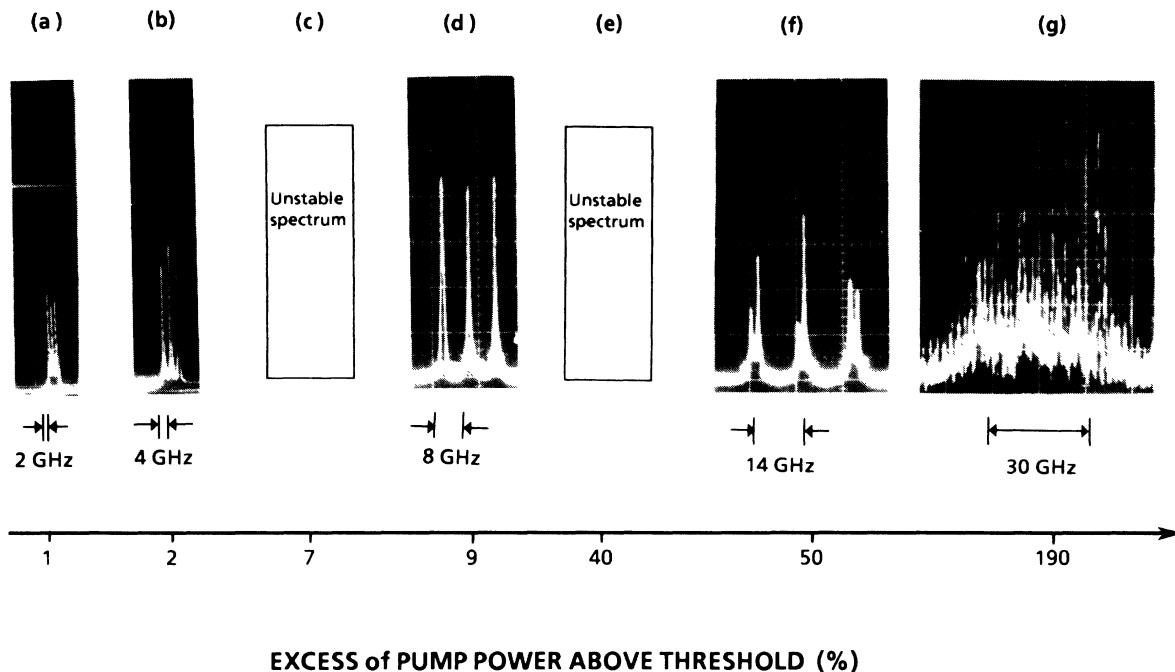


FIG. 2. Dye-laser optical spectrum as a function of excess of pump power above threshold.

denly jumps to 4 GHz [Fig. 2(b)]. Beyond a range of power where the spectrum is unstable, i.e., the mode intensities fluctuate [Fig. 2(c)], three stable modes again appear, now with spacing of 8 GHz [Fig. 2(d)]. Further increases in power lead eventually to a quasicontinuous spectrum, shown in Fig. 2(g), with a spectral width of about 100 cavity mode spacings and strongly fluctuating modes. We will discuss how the cavity configuration and alignment affect this behavior. We will show that the behavior in Figs. 2(a) and 2(b) can be well modeled by numerical simulations based on a third-order, coupled-mode laser theory, including the effects of spatial hole burning and an extremely weak étalon which arises spuriously from backscatter from the folding mirror in the cavity.

A study to determine the origin of the mode-intensity fluctuations in the unstable regions of Fig. 2 will be described. Our theoretical simulations with four-wave mixing and spatial hole-burning effects included show that the mode-intensity fluctuations arise even without spontaneous-emission noise present. Further, when four-wave mixing is omitted and spontaneous-emission noise is retained, no fluctuations are found. This leads us to conclude that the observed fluctuations in the laser are deterministic, and not driven by noise, either quantum or external. In the case of the experiment, the fluctuations are found to be deterministically chaotic, and hence are not noise driven. This was established by measuring the order-2 information dimension, which is found to be nonintegral, and the order-2 Kolmogorov entropy, which is found to be finite.

The correlation time of the mode intensity was measured and was found to decrease with increasing pump power. This is consistent with an earlier indirect measurement of the dependence of the mode "lifetime" on pump power.<sup>13</sup> The correlation time does not correspond to any obvious time constant of the system, but is correctly modeled by the numerical simulations. Our theory correctly predicts a decrease in mode correlation time with increasing pump power.

Finally, we will demonstrate that spatial hole burning<sup>30-32</sup> in the gain medium cannot be neglected in a correct model of the dynamics of the laser. Previous investigations have argued that spatial hole burning can be neglected in modeling this type of laser.<sup>2,11,16</sup>

## II. EXPERIMENT

### A. Laser

The configuration of the optical components of the dye laser studied in this experiment is shown in Fig. 1. The curved mirrors have standard dielectric, broadband, high-reflectivity coatings with a center wavelength of 590 nm. The output coupler is a Littrow prism with a standard 95% reflecting dielectric coating on the inner surface and no coating on the outer surface. This type of output coupler reduces the amount of specularly reflected light at the outer surface by virtue of its Brewster's angle with the optical axis of the cavity, and prevents reflected radiation from feeding back into the cavity. This design was essential because a standard output coupler, with a wedge angle of only a few minutes of arc, behaved as an

unwanted étalon. A single-plate birefringent tuner was used in the cavity to limit the spectral width of the laser. The tuner limited the bandwidth to a full width at half maximum of 30 GHz (100 cavity modes) at a pump power of 190% above threshold. The nominal threshold pump power was 135 mW.

The gain medium used was a ( $1 \times 10^{-3}$ )M solution of rhodamine 6G tetrafluoroborate dissolved in ethylene glycol, that flowed through the cavity in a jet. The jet was formed by a sapphire nozzle whose exit dimensions were 0.3 mm by 8.0 mm,<sup>33</sup> and lacked much of the high-frequency surface vibrations present in jets formed with conventional nozzles.<sup>34</sup> The dye solution was cooled to maintain constant viscosity, important for jet stability. Turbulence in the dye circulation system was minimized so that the frequency of bubbles flowing in the dye was less than one per second. The dye jet was pumped with a Spectra Physics 2020-05 argon-ion laser running on a single mode of the 514-nm line. We found that a multimode pump laser could affect the dynamics of the dye laser output.<sup>35</sup> An acousto-optic modulator in a feedback circuit with a bandwidth of 500 kHz was used to limit peak-to-peak intensity noise in the pump laser to less than 2%.

A laminar flow of dry nitrogen gas was introduced into a box that surrounded the dye laser. This aided in suppressing mechanical vibrations of the dye jet and laser cavity, due to turbulent air currents. It also eliminated dust in the atmosphere in the laser cavity. In order to obtain reproducible behavior it was essential to align carefully the laser to obtain pure TEM<sub>00</sub> operation. Only with this alignment could the stable spectra in Fig. 2 be clearly observed.

### B. Measurement apparatus

The output beam of the dye laser was allowed to propagate approximately 1 m before it impinged on any optical elements, to reduce the amount of backscattered radiation reaching the dye laser. To attenuate strongly any laser radiation that was reflected back toward the laser, the beam was first directed through a Faraday isolator. The isolator design is described in Ref. 36. Two plane-parallel Fabry-Pérot interferometers in series followed the isolator.

The first interferometer, operating in scanning mode, was used to obtain the optical spectra in Fig. 2. To measure to the intensity of a single mode, both Fabry-Pérots were required. The free spectral range of the first interferometer was 70 GHz. Their combined finesse was 2100. Since the cavity-mode spacing of the dye laser for this experiment was about 300 MHz, a single mode could be well resolved. The dye laser mode intensity that was transmitted through both interferometers was measured by a photodiode detector. For pump powers less than or equal to 110% above threshold the signal from this detector was digitized by a 12-bit analog-to-digital (AD) converter with a maximum digitization rate of 100 kHz. For higher pump powers, where the fluctuations are faster, an eight-bit transient digitizer with a maximum rate of 20 MHz was used. Those time series recorded with the AD converter were 10 000 samples long, while those obtained with the transient digitizer were limited to 4096 samples.

### C. Results

#### 1. Optical spectra

The optical spectra shown in Fig. 2 were obtained in the manner described in Sec. II B. The spectrum evolves by abrupt transitions as the pump power is varied. The three-peaked spectrum of Fig. 2(a), with a separation between adjacent peaks of 2 GHz, occurs at a pump power of approximately 1% above threshold. We call this type of spectrum “channeled,” and the behavior leading to it “channeling.” Increases in pump power result in no qualitative change in the spectrum, but simply a growth of the intensity of the individual peaks, until a critical power is reached at 2–5% above threshold. Then the outside peaks suddenly jump out to a separation of 4 GHz from the central peak. The unstable spectra [Figs. 2(c) and 2(e)] are composed of strongly fluctuating modes. In Fig. 2(g) the situation is similar, with the modes fluctuating on a faster time scale, which for the Fabry-Pérot scanning rate used yields the quasicontinuous spectrum shown. Increasing the pump power beyond approximately 110% of the threshold power results only in a broadening of this quasicontinuous spectrum. We found that the channeling behavior did not depend on the cavity length (cavity lengths from 38 to 70 cm were checked) or on the location of the birefringent tuner in the long arm of the cavity.

A 22-GHz radio-frequency (rf) spectrum analyzer was used in conjunction with a 10-GHz-bandwidth photodiode to obtain the power spectrum of the total laser intensity. This provided additional information about the mode structure of the channeled spectra. When the optical spectrum was as shown in Fig. 2(a) the intensity power spectrum of the dye laser consisted of two peaks, one at 2.019 GHz and a smaller peak at 4.038 GHz. This means that exactly three modes were lasing, separated by a frequency equal to seven times the cavity mode spacing, which was  $288.5(\pm 0.1)$  MHz. The intensity power spectrum of the dye laser corresponding to the optical spectrum of Fig. 2(b) was similar to that of Fig. 2(a), except that the two peaks were at 4.038 and 8.076 GHz. The modes of the channeled optical spectra in Figs. 2(a) and 2(b) are separated by the number of cavity modes closest to a multiple of 2 GHz. Recall that this behavior was not sensitive to changes of the cavity length. The intensities of single modes in the channeled spectra were measured and were found to be constant to within  $\pm 3\%$ . Hence these channeled spectra are composed of stable modes. Furthermore, the separation of peaks in all of the channeled spectra is a multiple of 2 GHz that is closest to an odd multiple of the spatial-hole-burning frequency (SHBF),  $c/4z_1$ , where  $z_1$  is shown in Fig. 1. For example, we did not observe a channeled spectrum with peak separation of 6 GHz. The SHBF for the cavity is 1.5 GHz, and a more complete discussion of its role in the laser's behavior will be given in Sec. III.

The principal source of the channelling can be traced to a weak étalon formed by the two curved cavity mirrors, which are separated by 7.5 cm (see Fig. 1). Light is backscattered toward the curved cavity end mirror from imperfections in the surface of the folding mirror. The

effective reflectivity of the folding mirror in the backward direction is determined by the amount of radiation that is scattered back into the  $TEM_{00}$  cavity mode. An étalon of this type will have almost unity transmission for all frequencies, with a slight sinusoidal modulation. The frequency separation between the maxima of this transmission function is given by  $c/2l$  where  $l$  is the distance between the folding mirror and the curved end mirror. This corresponds to a frequency of 2 GHz for this laser.

To verify that the separation of lasing modes in the channeled spectra depends on the distance between these mirrors, the 5-cm-radius end mirror was temporarily replaced with a 2.5-cm-radius mirror. The separation of the two curved mirrors was then 5 cm, giving a free spectral range of 3 GHz. The frequency separation between the modes of the channeled spectrum of the laser with this mirror was measured with the rf spectrum analyzer and was verified to be 3 GHz. The 5-cm end mirror was reinstalled for the remaining measurements of this study. We conclude that there exists a weak étalon with length equal to the distance between the two curved cavity mirrors. It may seem surprising that such a weak étalon can have a strong effect on the laser spectrum; however, this is to be expected since the high sensitivity of this type of laser has been demonstrated by intracavity spectroscopy. In Sec. III it will be shown that the channeling behavior can be modeled by assuming the presence of a weak étalon.

#### 2. Autocorrelation measurements of single modes

The intensities of single modes were measured, as described above, for the range of pump powers with unstable spectra [Figs. 2(c), 2(e), and 2(g)]. The fluctuations of the intensity of individual modes were found to be full scale at all pump powers measured, even though the total intensity was relatively constant. Figure 3 shows 1000 points of the intensity time series of individual modes of the dye laser, for two different pump powers. Figure 4 shows autocorrelation functions of the intensity time series corresponding to Fig. 3. The correlation time  $\tau_c$  of an individual mode was obtained by measuring the half width at half maximum of the central autocorrelation spike after subtracting the dc level. The resulting correlation times are plotted in Fig. 5. The trend of decreasing correlation time with increasing pump power is easily seen. This is related to two previously published results. Atmanspacher *et al.*<sup>13</sup> measured the effect of an absorber on the optical spectrum of a three-mirror dye laser and calculated the “mode lifetime” based on a simple model of ILS. In a recent paper Al'vazyan *et al.*<sup>17</sup> recorded on photographic film the intensity of a single mode from a two-mirror dye laser. From this a characteristic “fluctuation period” was inferred. Both groups reported a decrease of these characteristic time scales with pump power.

Also shown in Fig. 5 is the normalized variance of the fluctuations of the mode intensities. There is an inverse relation of the variance with the correlation time. At higher powers the mode intensity fluctuates more strongly.

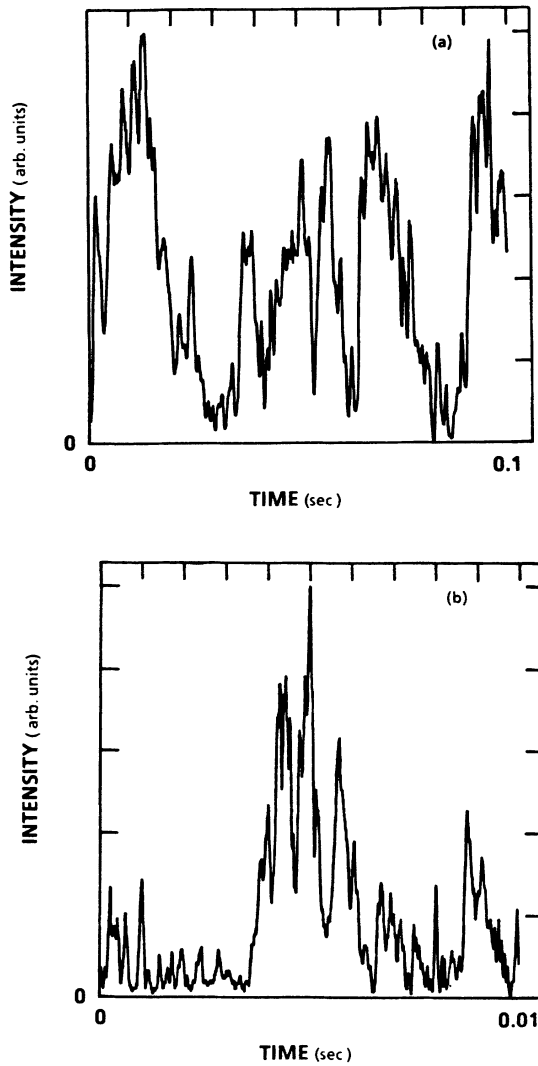


FIG. 3. Intensity vs time of the first 1000 points of recorded time series for the laser operating (a) in the region of Fig. 2(c), and (b) in the region of Fig. 2(e).

### 3. Deterministic chaos

The time series of the single-mode intensities were analyzed with a Grassberger-Proccacia numerical algorithm for determining the presence of deterministic chaos. A description of this method can be found in Refs. 37–39 and it is briefly described in Appendix A. In addition, Appendix A contains examples of how the algorithm was used to analyze the time series collected in this experiment. For all powers measured we found an estimate of the order-2 information dimension  $D_2$  of  $1.6 \pm 0.1$  (see Fig. 10 and Appendix A). The order-2 Kolmogorov entropy  $K_2$  was approximately 400 bits/sec at low power and increased to  $2 \times 10^5$  bits/sec at high power. The product  $K_2 \tau_c$  was approximately equal to unity at all powers, where  $\tau_c$  is shown in Fig. 5. This result suggests a fundamental relationship between  $K_2$  and  $\tau_c$ . To our knowledge this has not been explored theoretically.

$D_2$  and  $K_2$  are measures of a phase-space attractor of a

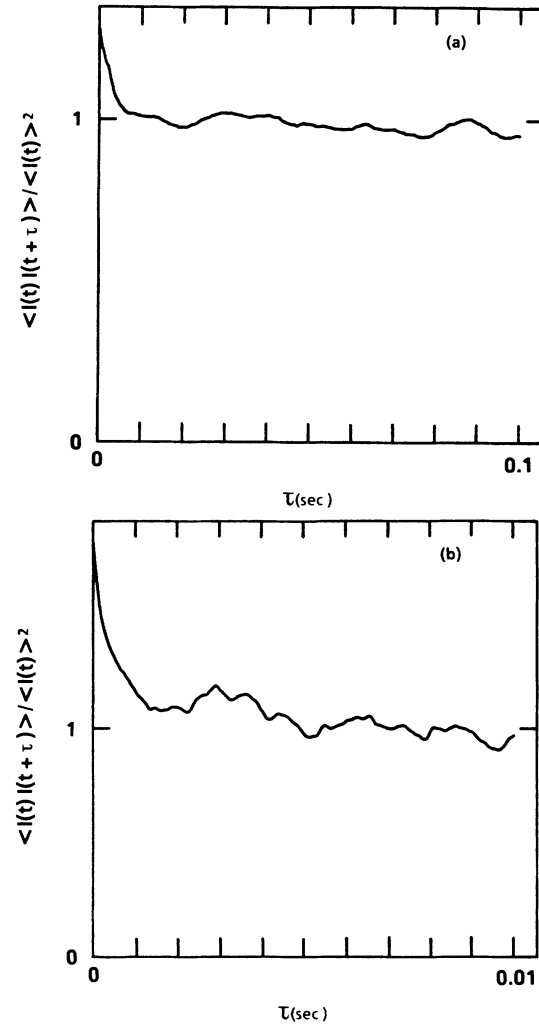


FIG. 4. Intensity autocorrelation functions of the full time series corresponding to (a) Fig. 3(a); (b) Fig. 3(b).

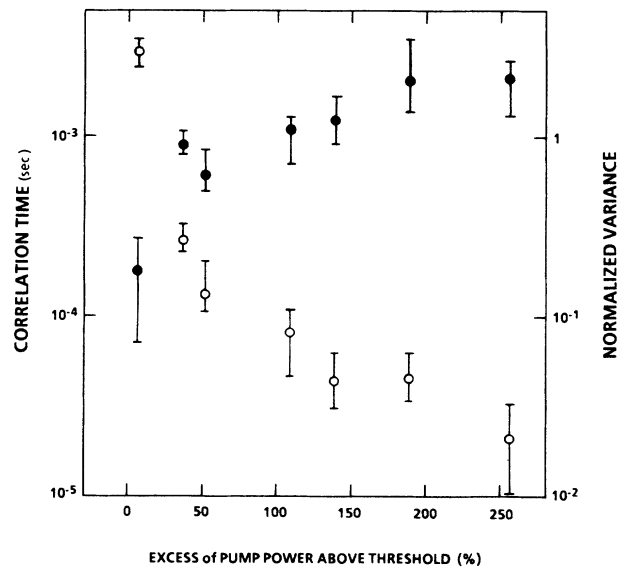


FIG. 5. Correlation time  $\tau_c$  ( $\circ$ ) and normalized variance  $(\langle I^2 \rangle - \langle I \rangle^2) / \langle I \rangle^2$  ( $\bullet$ ) of a single-mode intensity from the multimode laser output. The error bars represent the spread of three to five measurements.

dynamical system.  $D_2$  is a lower bound of the capacity  $D$ , which is a geometric measure of the attractor.<sup>40</sup>  $K_2$  is a lower bound of the Kolmogorov entropy  $K$ ,<sup>40</sup> which is a measure of the rate of loss of information about the state of a dynamical system.<sup>41</sup> A chaotic attractor will have a value of  $D$  which is noninteger and a nonzero, finite value of  $K$ . In addition, the intensity power spectrum of a chaotic signal is continuous. The intensity power spectra of the single-mode intensities were calculated numerically using a fast-Fourier-transform algorithm and were found to be continuous. This analysis means that the fluctuations of the single-mode intensities are deterministically chaotic. Atmanspacher *et al.* have also found evidence of deterministic chaos in a similar laser by measuring the sum intensity of many adjacent modes.<sup>15</sup>

### III. THEORY

#### A. Equations of motion

We have found that many features of this laser's behavior can be described by semiclassical, third-order laser theory. This theory includes the effects of population oscillations, four-wave mixing among the lasing modes, and spatial hole burning due to the standing-wave nature of the cavity. Since at all powers studied the optical and rf spectra indicated narrow-band (<200 kHz) frequency components, a decomposition of the total field into spatial modes, each with a well-defined temporal frequency should be valid. The equations for the time-dependent mode amplitudes  $A_l(t)$  are

$$\begin{aligned} \frac{d}{dt} A_l(t) = & \left[ -\gamma_l + g - \frac{3ga}{4\gamma} |A_l(t)|^2 - \frac{ga}{2} \sum_{n \neq l} |A_n(t)|^2 C_{nl} \left[ \frac{1}{\gamma} + \frac{1}{\gamma + i\Delta_{nl}} \right] \right] A_l(t) \\ & - \frac{ga}{2} \sum_{j \neq n} \sum_n A_n(t) A_j^*(t) A_{l-n+j}(t) \frac{C_{lnj}}{\gamma + i\Delta_{nl}} + F_l(t), \end{aligned} \quad (1)$$

and they are derived in Appendix B. In this set of coupled equations,  $\gamma_l$  is the cavity decay rate of mode  $l$  and  $g$  is the gain coefficient. The third term corresponds to self-saturation. In this term  $a$  is determined by the dipole matrix element of the assumed two-level lasing transition and by the off-diagonal relaxation rate;  $\gamma$  is the diagonal relaxation rate. The fourth term corresponds to mode competition, the fifth term represents four-wave mixing, and  $F_l(t)$  is a Langevin noise source.  $C_{nl}$  and  $C_{lnj}$  are coupling coefficients and are given by Eqs. (B13) and (B16) in Appendix B;  $\Delta_{nl}$  is the angular frequency difference between modes  $n$  and  $l$ . The Langevin term  $F_l(t)$  is used to describe spontaneous emission and has the correlation properties<sup>22,23</sup>

$$\langle F_l(t) \rangle = 0 \quad (2a)$$

and

$$\langle F_l(t) F_l^*(t') \rangle = \frac{16\pi}{V} \hbar \omega_l \gamma_l \delta_{ll'} \delta(t-t'), \quad (2b)$$

where  $V$  is the effective cavity-mode volume,  $\pi w^2 L$ , where  $L$  is the cavity length and  $w$  is the radius of the mode in the gain medium ( $\sim 10 \mu\text{m}$ ).

The effects of spatial hole burning are contained in the coupling coefficients.  $C_{nl}$  is a measure of the spatial overlap of the standing-wave modes  $n$  and  $l$  within the gain medium. This coefficient has the property  $\frac{1}{2} \leq C_{nl} \leq \frac{3}{2}$ .  $C_{nl}$  attains its minimum value when the two standing-wave modes are spatially  $90^\circ$  out of phase with each other inside the gain medium; thus the nodes of one mode overlap the antinodes of the other, and the two modes will not compete strongly for gain. This occurs when the two modes are separated in frequency by an odd multiple of  $c/4z_1$ , the spatial-hole-burning frequency, where  $z_1$  is the distance from the gain medium to the closest cavity end mirror, as illustrated in Fig. 1. This effect is not as im-

portant in lasers with a gain medium which takes up a significant fraction of the cavity length, as the modes will not maintain a constant phase relation throughout the gain medium.<sup>12</sup> In the laser we are studying, however, the gain medium is very thin and spatial hole burning can dramatically affect the laser dynamics.

#### B. Numerical solutions

We have numerically solved Eqs. (1) using parameters that correspond to those of our laser. In our simulations we have included 31 modes, which is sufficient to model fully the behavior described in regions corresponding to Figs. 2(a) and 2(b). We have used  $\gamma = 5 \times 10^8 \text{ sec}^{-1}$ ,  $a = 1.1 \times 10^5 \text{ cm}^3 (\text{erg sec})^{-1}$ , and  $g$  was varied, with a value of  $8.7 \times 10^6 \text{ sec}^{-1}$  at 1% above laser threshold. The cavity parameters used in the simulations were  $z_1 = 5 \text{ cm}$  (see Fig. 1), a cavity length  $L = 52 \text{ cm}$ , and a gain medium thickness of  $\delta z = 400 \mu\text{m}$ . In Sec. II we discussed the effects of backscattering of radiation from the cavity folding mirror, noting that it causes a weak étalon with a free spectral range of 2 GHz. We have incorporated the effects of this étalon into the individual cavity mode loss rates  $\gamma_l$ . The minimum loss rate is  $\gamma_0 = 8.6 \times 10^6 \text{ sec}^{-1}$ , corresponding to the center mode, and we have taken the relative modulation strength of the cavity-mode loss rates to be  $6 \times 10^{-4}$ . This strength is within an order of magnitude of an estimate of this effect, and was chosen to model properly the experimental observations. We have also included the effects of the bandwidth-limiting birefringent tuner into our estimate of the cavity-mode loss rates. We took this tuner to impose a parabolic shaped loss which increases with the frequency separation from the center mode. We have used a relative increase of  $3 \times 10^{-5}$  for the two modes that are farthest from the center mode. The initial conditions for our simulations are obtained from a random number genera-

tor, with a Gaussian distribution for the complex mode amplitudes.

### 1. Optical spectrum

Numerical results for the laser operating 1% and 3% above threshold are shown in Figs. 6(a) and 6(b), respectively. For these solutions we have taken  $F_l(t)=0$ . Intensities  $|A_l(t)|^2$  of 15 of the 31 modes in the simulation are plotted as a function of time. The 16 unplotted modes behave much the same as those plotted modes

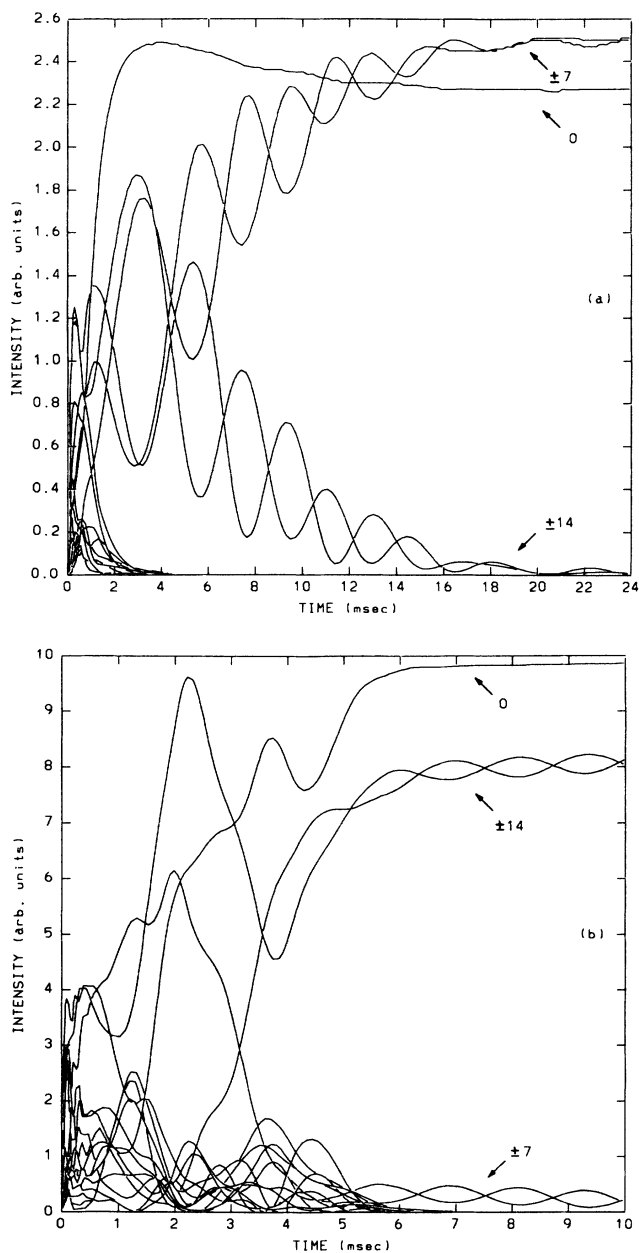


FIG. 6. Solutions of Eqs. (1) for intensity vs time of 15 of the 31 calculated laser modes, with 5 of the modes identified by the number of mode spacings from the center mode (mode 0). The parameters correspond to a laser operating (a) 1% above threshold ( $g=8.7 \times 10^6 \text{ sec}^{-1}$ ) and (b) 3% above threshold ( $g=8.9 \times 10^6 \text{ sec}^{-1}$ ).

which are seen to die out after a few milliseconds. In Fig. 6(a) we see that the stationary solution consists of three dominant modes. Mode 0 is the center mode, while modes  $\pm 7$  are each spaced 2 GHz from the center mode and are seen to have a slightly higher intensity. Thus we see that the spectrum obtained from this solution matches the experimental spectrum of Fig. 2(a) very well. In Fig. 6(b), we see that when the gain coefficient is increased, modes  $\pm 14$  become the dominant side modes. These modes are separated from the center mode by 4 GHz, and the center mode has the strongest intensity, so the spectrum of this solution agrees with the experimentally obtained spectrum shown in Fig. 2(b).

It will be demonstrated below that the combined effects of spatial hole burning and four-wave mixing are responsible for this sudden jump in the laser spectrum. This behavior can be explained as follows. The observed separation of the lasing modes in the lower power region is 2.019 GHz, whereas it is 4.038 GHz in the higher power region. Since the SHBF for this laser is 1.5 GHz, 4.038 GHz is closer to three times the SHBF than 2.019 is to one times the SHBF. This means that the 4-GHz modes are the preferred modes according to spatial-hole-burning arguments. At low pump powers, the effect of the birefringent tuner is to suppress more strongly modes that are farther from the center laser frequency. As the laser power is raised, the third-order terms in Eqs. (1) which correspond to spatial hole burning and four-wave mixing become more important. Spatial hole burning then allows the modes farther from line center to lase, despite the fact that they have higher losses. Spatial hole burning presents the necessary conditions that allow the four-wave mixing interaction of the lasing modes to drive the system to lase with larger frequency separation. However, the effect of spatial hole burning is not strong enough to overcome the effect of the backscattering étalon, and that is why lasing occurs at multiples of the étalon frequency.

Notice in Fig. 6(a) that the spectrum condenses to five modes after 4 msec, whereas at the higher power in Fig. 6(b) this occurs after 6 msec. This trend continues to higher powers. When the pump power is increased to 7% above threshold the solution shown in Fig. 7 is obtained, where again we have taken  $F_l(t)=0$ . The transient behavior persists for 32 msec before the spectrum condenses. For clarity Fig. 7(a) shows only 5 of the 31 laser modes plotted as a function of time. In the transient region the other 26 modes have the same fluctuating behavior and approximately the same average intensity as the plotted modes. In the stationary region the unplotted modes have no significant intensity. It is interesting to note that the sum of the calculated mode intensities was constant to within 0.02%, even though the individual modes were strongly fluctuating. Figure 7(b) shows the time behavior of the center mode under the same conditions as in Fig. 7(a). The percentage above threshold in Fig. 7 corresponds roughly to the region of Fig. 2(c) in our experimental study, and the full-scale mode-intensity fluctuations that we see in the transient region, Fig. 7(b), bear a remarkable resemblance to the fluctuations we see experimentally at this power level, Fig. 3(a). Note that

this solution is in the absence of any stochastic driving terms.

## 2. Fluctuation dynamics

From the time series of Fig. 7(b) we have calculated a correlation time of 1 msec, using the same procedure as was used for the experimental data. This agrees fairly well with the experimentally measured correlation time of 2.5 msec. Note that this time scale is much longer than any time scale that can be simply deduced from the

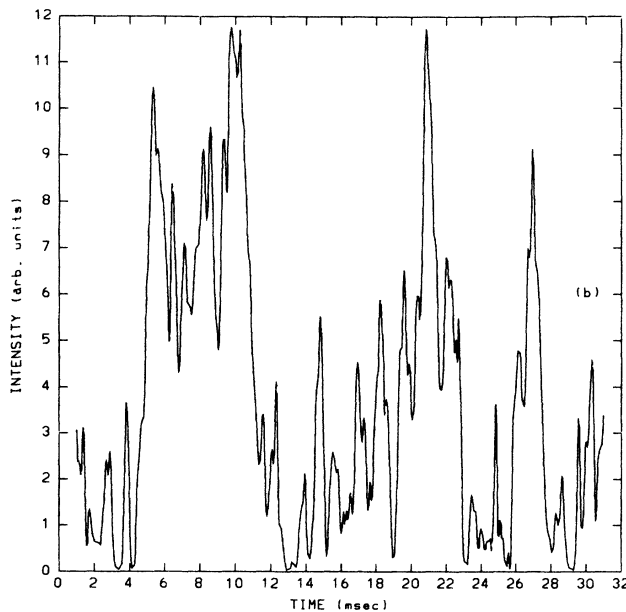
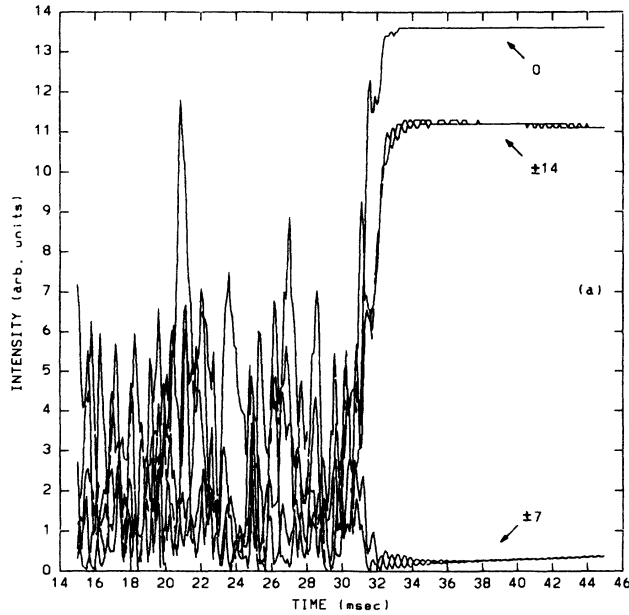


FIG. 7. (a) Solutions of Eqs. (1) for intensity vs time of 5 of the 31 calculated laser modes, with the modes identified. The parameters correspond to a laser operating 7% above threshold ( $g = 9.3 \times 10^6 \text{ sec}^{-1}$ ). (b) Intensity vs time of the center lasing mode (mode 0) under the conditions of (a).

values of the parameters appearing in Eqs. (1).

We have increased the pump power in our simulations to as high as 12% above threshold and have found that the time scale of the mode intensity fluctuations decreases with increasing pump power. At these higher powers we do not have long enough time series to determine accurately the correlation times, due to computing time limitations, but we do find the general trend of decreasing correlation times with increasing pump power, which is in agreement with the experiment (see Fig. 5). In the numerical simulations we have included 31 modes. This is insufficient to model completely the laser behavior at pump powers greater than or equal to 7% above threshold. As the pump power is increased more modes exceed threshold, due to the effect of the birefringent tuner. The limited number of modes in our model may be why the theoretical results eventually reach steady state, whereas none is observed in the experiment. In order to do a more accurate simulation we would have to double the number of modes, and this is impractical in terms of computing time.

In the solutions of Eqs. (1) discussed so far, the quantum noise term  $F_i(t)$  was neglected. Previous treatments had considered quantum noise to be responsible for the mode-intensity fluctuations.<sup>3,5,7</sup> But note that our solution (Fig. 7) at 7% above threshold displays large fluctuations without any added stochastic noise. We have checked our solutions for stability with respect to additive quantum noise for pump powers greater than 1% above threshold. (For lower pump powers the fluctuations are found experimentally to be dominated by pump noise.) It was found theoretically that the addition of quantum noise in the transient region affected the exact time evolution of the system, as shown in Fig. 8. In this figure we show the results of two different simulations,

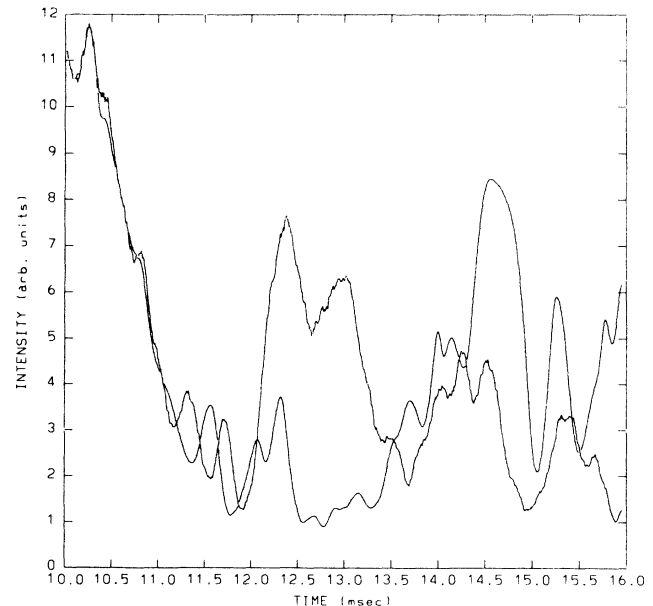


FIG. 8. Intensity vs time of single mode (mode 0) of the 31 calculated laser modes plotted for simulations with and without added quantum noise. All other parameters correspond to those of Fig. 7.

one with added quantum noise and one without. The noise was added starting at 10 msec, and we see that the two solutions are initially the same, but that the noise causes them to diverge. However, the time scales of the fluctuations both with and without noise are the same, except for the presence of small, fast noise in the former case. It was also found that the addition of noise did not

In an attempt to determine whether quantum noise, without four-wave mixing present, can give rise to the fluctuating behavior in our laser, we altered Eqs. (1) to eliminate the effects of population oscillations, and thus of four-wave mixing. This is strictly valid only for  $\Delta_{nl} \gg \gamma$ . Since in our laser  $\gamma = 5.0 \times 10^8 \text{ sec}^{-1}$  and the smallest value of  $\Delta_{nl}$  is  $1.8 \times 10^9 \text{ sec}^{-1}$ , this is not strictly valid, but we do it as a formal procedure for comparison to the full equations (1). In this limit Eqs. (1) become

$$\frac{d}{dt} A_l(t) = \left[ -\gamma_l + g - \frac{3ga}{4\gamma} |A_l(t)|^2 - \frac{ga}{2\gamma} \sum_{n \neq l} |A_n(t)|^2 C_{nl} \right] A_l(t) + F_l(t). \quad (3)$$

This is often called the free-running approximation,<sup>3,12,22</sup> and, in the absence of the noise term, Eqs. (3) are equivalent to those that one would get in the limit of photon rate equations. The most important difference between these equations and Eqs. (1) is the absence of the four-wave mixing terms.

We have numerically solved Eqs. (3) with the noise term  $F_l(t)$  included and all other parameters the same as used for the solutions shown in Fig. 7. The results are shown in Fig. 9. The irregular behavior seen in Fig. 7 is

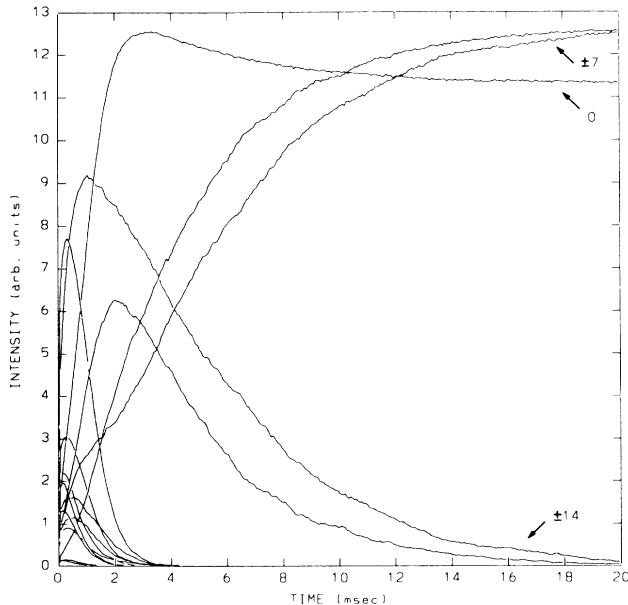


FIG. 9. Solutions of free-running-approximation equations (3) for intensity vs time of 15 of the 31 calculated laser modes, with 5 of the modes identified. The parameters correspond to the laser operating 7% above threshold ( $g = 9.3 \times 10^6 \text{ sec}^{-1}$ ).

completely absent in the solutions of Eqs. (3). This indicates that four-wave mixing is required in the realistic model of our laser in order to obtain fluctuations.

The solution of Eqs. (3) also indicates the origin of the spectral instability discussed in Sec. II. To make a more direct comparison with the solution shown in Fig. 7 we have also solved Eqs. (3) without quantum noise, and obtained essentially the same result as with quantum noise shown in Fig. 9. Note that the stationary state obtained is not the same as that with four-wave mixing included (Fig. 7). The comparison of these solutions indicates that four-wave mixing is necessary for the spectral instability in Figs. 2(a) and 2(b) to occur.

It was recently argued by Aĭvazyan *et al.* that the fluctuation of the individual mode intensities is due to a nonlinear interaction between the cavity modes.<sup>17</sup> The model used by Aĭvazyan *et al.* is based upon stochastic photon rate equations, with terms representing stimulated Brillouin scattering added. Thus it necessarily leaves out all effects in the laser which depend on the field nature of light (i.e., four-wave mixing). We have found here that the nonlinear interactions between modes arising naturally from four-wave mixing gives rise to fluctuations without assuming the presence of other processes, such as Brillouin scattering.

### 3. Deterministic chaos

Due to the short duration of the theoretical time series [Fig. 7(b)] no meaningful results can be obtained from a Grassberger-Procaccia calculation of the order-2 information dimension and the Kolmogorov entropy. The short duration of the time series also limited the resolution of the calculated intensity power spectrum to 100 Hz. No clear evidence of periodicity was found. Again, in order to better model the experiment the number of modes would have to be doubled, greatly increasing the computing time.

## IV. CONCLUSIONS

We have found four-wave mixing (FWM) and spatial hole burning (SHB) to be the root of much of the laser behavior we have discussed. These processes are responsible for the deterministic fluctuations of mode intensities, and coupled with the weak étalon, they produce the optical spectra observed. We found that the fluctuations of the intensities of individual modes are deterministically chaotic with an estimate of the order -2 information dimension  $D_2$  of  $1.6 \pm 0.1$ . In addition, we found that order -2 Kolmogorov entropy was always approximately equal to the inverse of the single-mode-intensity correlation time  $\tau_c$ , i.e.,  $K_2 \tau_c \approx 1$ . The significance of this result is not presently understood. We have found that SHB and FWM cause the abrupt transitions in the distribution of lasing modes, as the pump power is increased. Thus they drive the system to have a broader spectrum as the pump power is increased, subject to the static constraints of the weak étalon and the birefringent tuner. This instability may be the cause of the discrete jumps in "power spectral density" observed by Atmanspacher *et al.*<sup>14,16</sup>

We have shown that a semiclassical third-order laser

theory, including FWM, is successful in modeling a variety of experimental observations, and that stochastic photon rate equations do not correctly model the laser. The full-scale fluctuations driven by FWM are found theoretically to have correlation times that decrease with increasing power, as has been well documented by our experiment and others.<sup>13,17</sup> Further, we found that the time period for which the numerical solutions were strongly fluctuating increases as the pump power is increased. This may explain why at certain pump powers (for which we cannot obtain numerical solutions of our full model) a stationary state is not observed in the experiment. The transient regime may be sufficiently long ( $\sim 1$  sec) that the laser is always perturbed before it can reach a stationary state. Why FWM can dominate additive quantum noise in producing the fluctuations of the laser mode intensities can be partially understood by the following heuristic argument. SHB allows more than one mode to lase simultaneously; this means that FWM will always be present. Thus, as the pump power is increased above threshold, the fifth term in Eqs. (1) will have a larger magnitude than will the additive quantum noise.

From a practical perspective the channeling behavior we observe is surprising; the spectral instabilities that occur are more complicated than the laser behavior that might be expected from the influence of a weak étalon. From a theoretical perspective one may wonder why such a laser displays a rich array of instabilities at pump powers at very small (3%) excess above lasing threshold. This is in contrast with the theoretically well-known Lorenz instability, which was predicted by Haken in 1975 to occur in a single-mode, homogeneously broadened ring laser at about nine times above threshold.<sup>42</sup> The simple answer is that in the multimode, standing-wave, homogeneously broadened laser the effect of spatial hole burning decouples the modes to a certain extent, creating more independent degrees of freedom than are found in the single-mode, homogeneously broadened, ring laser. It is not surprising, but also not always true, that the system with the larger number of degrees of freedom can display instabilities at lower pump powers. This type of result

has also been observed in lasers with inhomogeneous broadening of the gain transition.<sup>43,44</sup> In this case, the degrees of freedom correspond to different velocity groups.

It should be pointed out that the instabilities that we observe are not related directly to those studied by Hillman *et al.*<sup>45,46</sup> In that case the laser cavity was a ring and the optical field strength was so high that the Rabi frequency was comparable to the homogeneous medium linewidth. In our laser this was not the case.

Finally, we believe that the spectral channeling behavior that we have observed is generic to three-mirror-cavity lasers with thin, homogeneously broadened gain media. This may adversely affect their application to intracavity spectroscopy.

#### ACKNOWLEDGMENTS

We wish to thank Z. Deng and F. T. Hioe for very useful discussions and collaborations. We also thank D. J. Gauthier and T. H. Chyba for many helpful discussions on deterministic chaos. This work was supported by the U. S. Department of Energy, Office of Basic Energy Sciences, Chemical Sciences Division. The numerical computations were carried out using the supercomputer at the John von Neumann Center, a consortium of which the University of Rochester is a member.

#### APPENDIX A

In this appendix we describe the data analysis carried out to estimate  $D_2$  and  $K_2$  of a chaotic attractor from a time series of the single-mode intensity of the laser and give examples of its application on two of the time series analyzed.

We use an algorithm developed by Grassberger and Procaccia that reconstructs the attractor in a  $d$ -dimensional embedding space. This procedure is discussed in Refs. 37–39 and will only be briefly outlined here. A time series  $[I(t_i)]$ , is obtained by digitizing the single-mode intensity. From this time series, vectors with components

$$\{I(t_i), I(t_i + m\tau), I(t_i + 2m\tau), I(t_i + 3m\tau), \dots, I(t_i + dm\tau)\}$$

are formed. The time between samples is  $\tau$  and  $m$  is the embedding delay. A correlation sum  $C_d(l)$  is obtained by calculating the Euclidean norm of all possible pairs of vectors of dimension  $d$  and counting the number of pairs of vectors with norm less than  $l$ . Examples of  $\ln[C_d(l)]$  versus  $\ln(l)$  are shown in Figs. 10(a) and (b). One looks for a set of  $\ln[C_d(l)]$  with successive values of  $d$  which, for a range of  $l$ , becomes a series of straight and parallel lines with constant separation. For example, in Figs. 10(a) and 10(b) this occurs at around  $\ln(l)=5$ . Then an estimate for  $D_2$  and  $K_2$  for a chaotic attractor can be obtained from<sup>37</sup>

$$\ln[C_d(l)] = D_2 \ln(l) - d\tau K_2 + \text{const.}$$

$D_2$  is the slope of the straight-line segments and  $\tau K_2$  is

their separation. If a signal is dominated by noise, then the slope and the separation of straight-line segments of  $\ln[C_d(l)]$  increases with increasing values of  $d$ . Thus  $D_2$  and  $\tau K_2$  scale with embedding dimension. For a periodic signal,  $D_2$  is an integer and  $K_2$  is zero.

Figure 10(a) shows the  $\ln[C_d(l)]$  curves for a 10 000-point time series of the intensity fluctuations of single mode of the dye laser at 7% above threshold. The  $\ln[C_d(l)]$  curves for a 4096-point time series 186% above threshold are shown in Fig. 10(b). The digitization sampled time  $\tau$  was chosen to ensure that a typical oscillation period was sampled by approximately 50 points [ $\tau=10^{-4}$  sec and  $2 \times 10^{-5}$  sec for Figs. 10(a) and (b) respectively]. The value of  $m$  was chosen to make  $m\tau$  approximately equal to the delay time at which the autocorrelation function of the time series no longer decreases monotonically.

This causes the vectors compared in the analysis to be more nearly linearly independent than would be the case for  $m = 1$ . The maximum embedding dimension in the calculation of  $C_d(l)$  of Fig. 10(a) is 25 and  $m$  is taken to be 100. These values resulted in a total of 7475 vector comparisons. For Fig. 10(b) the maximum  $d$  was 20 and  $m = 60$ , resulting in a 2876-vector comparison. In both Figs. 10(a) and 10(b) the slope and the separation of the straight-line segments of  $\ln[C_d(l)]$  saturate for  $d$  greater than 12. We find a value for  $D_2$  of 1.6 for Fig. 10(a) and 1.5 for Fig. 10(b). In each case  $K_2$  goes to a finite value, as discussed in the text.

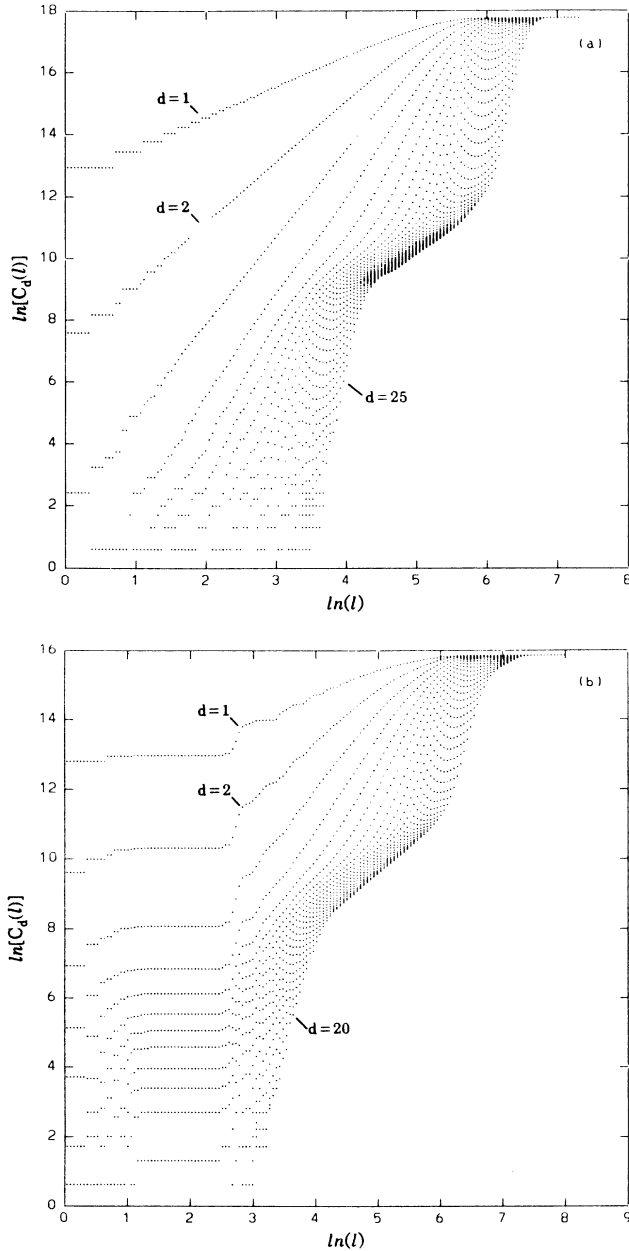


FIG. 10. Plots of the natural logarithm of the correlation sum  $\ln[C_d(l)]$  vs  $\ln(l)$  for (a) 10000-point time series of the laser intensity at a pump power 7% above threshold, and (b) 4096-point time series of the laser intensity at a pump power 186% above threshold.

## APPENDIX B

In this appendix we will derive Eqs. (1) of the text. We will use as a starting point the Maxwell-Bloch equations. We assume that the lasing transition can be treated as a two-level system with upper state  $|2\rangle$ , lower state  $|1\rangle$ , density operator  $\hat{\rho}$ , and an energy difference between the two levels of  $\hbar\bar{\omega}$ . The optical Bloch equations of motion of the two-level system in the rotating frame are

$$\frac{d}{dt}S(z,t) = -\beta S(z,t) - \frac{id}{\hbar}E(z,t)W(z,t), \quad (\text{B1a})$$

$$\begin{aligned} \frac{d}{dt}W(z,t) = & -\gamma(W(z,t) - W_0) + \frac{id}{2\hbar}S^*(z,t)E(z,t) \\ & - \frac{id^*}{2\hbar}S(z,t)E^*(z,t), \end{aligned} \quad (\text{B1b})$$

where  $S(z,t) = \langle 1 | \hat{\rho} | 2 \rangle \exp(-i\bar{\omega}t)$  is the dipole coherence and  $W(z,t) = \langle 2 | \hat{\rho} | 2 \rangle - \langle 1 | \hat{\rho} | 1 \rangle$  is the population inversion of the system, with equilibrium value  $W_0$  in the absence of lasing. In Eqs. (B1)  $\beta$  is the dipole dephasing rate,  $\gamma$  is the population decay rate of the upper level, and  $d$  is the transition dipole moment.  $E(z,t)$  is the amplitude of the positive-frequency component of the total electric field  $\epsilon$ , i.e.,  $\epsilon = \frac{1}{2}E(z,t)\exp(-i\bar{\omega}t) + \text{c.c.}$

In addition to the Bloch equations, we use the wave equation

$$\left[ \frac{\partial^2}{\partial z^2} - \frac{1}{c^2} \frac{\partial^2}{\partial t^2} \right] E(z,t)e^{-i\bar{\omega}t} = \frac{\partial^2}{\partial t^2} \frac{4\pi}{c^2} N_0 d S(z,t)e^{-i\bar{\omega}t}, \quad (\text{B2})$$

where  $N_0$  is the number density of active molecules in the gain medium. Since we are interested in the behavior of individual modes of the laser field, we will expand the field in terms of the spatial modes  $u_l(z)$  of the cavity

$$E(z,t) = \sum_l A_l(t) u_l(z) e^{-i\Delta_l t}, \quad (\text{B3})$$

where  $A_l(t)$  is the amplitude of the  $l$ th cavity mode,  $\Delta_l = \omega_l - \bar{\omega} = l\Delta$ ,  $\omega_l$  is the bare-cavity frequency of mode  $l$ , and  $\Delta = \pi c/L$  with  $L$  being the laser cavity length. The mode functions of the standing-wave cavity are  $u_l(z) = \sin(k_l z)$ , where  $k_l = \omega_l/c$ .

It is found in a dye laser that the mode amplitudes  $A_l(t)$  vary on a time scale that is much longer than  $\bar{\omega}^{-1}$ . Using this fact and the orthogonality of the mode functions, we substitute Eq. (B3) into Eq. (B2) to find the equations for the individual mode amplitudes  $A_l(t)$ ,

$$\frac{d}{dt}A_l(t) = i2\pi\bar{\omega}N_0 d e^{i\Delta_l t} \frac{2}{L} \int_{z_1}^{z_1+\delta z} u_l(z) S(z,t) dz. \quad (\text{B4})$$

In a dye laser operating at low powers, the dipole dephasing occurs on a much shorter time scale than any other process in the system; thus we may adiabatically eliminate the coherence  $S(z,t)$  from our problem. With this approximation,  $S(z,t)$  is found from Eq. (B1a) to be

$$S(z,t) \simeq \frac{-idE(z,t)W(z,t)}{\hbar\beta}. \quad (\text{B5})$$

Combining Eqs. (B1b), (B3), (B4) and (B5), we obtain the differential equations for the mode amplitudes and the inversion<sup>47</sup>

$$\frac{d}{dt} A_l(t) = -\gamma_l A_l(t) + b \sum_n A_n(t) e^{-i\Delta_{nl}t} \int_{z_1}^{z_1+\delta z} u_l(z) u_n(z) W(z,t) dz, \quad (\text{B6a})$$

$$\frac{d}{dt} W(z,t) = -\gamma [W(z,t) - W_0] - a W(z,t) \sum_{l,n} A_l(t) A_n^*(t) u_l(z) u_n(z) e^{i\Delta_{nl}t}. \quad (\text{B6b})$$

In Eqs. (B6),  $\gamma_l$  is the cavity decay rate of mode  $l$ ,  $\Delta_{nl} = (n-l)\Delta$ , and  $a = (d^2)/(\hbar^2\beta)$ . The parameter  $b$  is given by

$$b = \frac{4\pi N_0 \bar{\omega} d^2}{\hbar L \beta}. \quad (\text{B7})$$

The integration in Eqs. (B6a) is over the cavity gain medium, where  $z_1$  is the distance from the gain medium to the closest cavity end mirror and  $\delta z$  is the thickness of the medium.

Equations (B6) will be written in third-order, perturbative form by expanding the inversion around the equilibrium value. Assuming that the population oscillates at the intermode beat frequencies, then

$$W(z,t) = W_0 + \sum_k W_k(z,t) e^{ik\Delta t} \quad (k=0, \pm 1, \pm 2, \dots). \quad (\text{B8})$$

We assume that the amplitudes of the Fourier coefficients  $W_k(z,t)$  do not change much on a time scale of  $\Delta^{-1}$ . This means that

$$\frac{d}{dt} W_k(z,t) \simeq \sum_k ik\Delta W_k(z,t) e^{ik\Delta t}. \quad (\text{B9})$$

Substituting (B8) and (B9) into (B6b) and assuming  $W_0 \gg W_k(z,t)$ , we equate coefficients of the different Fourier components and find

$$W_k(z,t) = -\frac{aW_0}{ik\Delta + \gamma} \sum_j A_{j-k}(t) A_j^*(t) u_{j-k}(z) u_j(z). \quad (\text{B10})$$

We want to substitute Eqs. (B8) and (B10) into (B6a) to get the differential equations for the mode amplitudes; however, we must be self-consistent with the assumptions that we have made so far. The assumption that the Fourier coefficients  $W_k(z,t)$  vary little on a time scale of  $\Delta^{-1}$  implies that the mode amplitudes  $A_l(t)$  will also be approximately constant over this time interval. Therefore, when we substitute Eqs. (B8) and (B10) into (B6a), we must keep only those terms that are approximately constant over a time  $\Delta^{-1}$ . Doing this we obtain the equations

$$\frac{d}{dt} A_l(t) = (-\gamma_l + g) A_l(t) - \frac{ga}{2} \sum_j \sum_n A_n(t) A_j^*(t) A_{l-n+j}(t) \frac{C_{lnj}}{\gamma + i\Delta_{nl}} + F_l(t), \quad (\text{B11})$$

where we have used the fact that for a gain medium that is many wavelengths thick

$$\int_{z_1}^{z_1+\delta z} u_l^2(z) dz \simeq \frac{\delta z}{2}, \quad (\text{B12})$$

and we have made the definitions  $g = (W_0 b \delta z)/2$  and

$$C_{lnj} = \frac{4}{\delta z} \int_{z_1}^{z_1+\delta z} u_l(z) u_n(z) u_j(z) u_{l-n+j}(z) dz. \quad (\text{B13})$$

In a dye laser the gain bandwidth is much broader than the laser bandwidth, so we may take  $g$  to be constant for all modes. In Eqs. (B11) we have added the Langevin noise term  $F_l(t)$ , which when used to describe spontaneous emission has the properties given in Eqs. (2). Equations (B11) are in the form that is most easily solved on a computer.

We will rewrite Eqs. (B11) in a form that yields more physical insight. If we take out the  $n=l$  and  $j=n$  terms from the double summation we obtain Eqs. (1) of the text:

$$\begin{aligned} \frac{d}{dt} A_l(t) = & \left[ -\gamma_l + g - \frac{3ga}{4\gamma} |A_l(t)|^2 - \frac{ga}{2} \sum_{\substack{n \\ n \neq l}} |A_n(t)|^2 C_{nl} \left( \frac{1}{\gamma} + \frac{1}{\gamma + i\Delta_{nl}} \right) \right] A_l(t) \\ & - \frac{ga}{2} \sum_{\substack{j \\ j \neq n \\ n \neq l}} \sum_n A_n(t) A_j^*(t) A_{l-n+j}(t) \frac{C_{lnj}}{\gamma + i\Delta_{nl}} + F_l(t), \end{aligned} \quad (\text{B14})$$

where we have defined  $C_{llj} = C_{ljj} = C_{lj}$ , i.e.,

$$C_{lj} = \frac{4}{\delta z} \int_{z_1}^{z_1+\delta z} u_l^2(z) u_j^2(z) dz. \quad (\text{B15})$$

In the usual case that the gain medium is many wavelengths thick  $C_{ll} \simeq \frac{3}{2}$ , and

$$C_{ij} \simeq 1 + \frac{1}{\frac{4\pi}{L}(l-j)\delta z} \left[ \sin \left[ \frac{2\pi}{L}(l-j)(z_1 + \delta z) \right] - \sin \left[ \frac{2\pi}{L}(l-j)z_1 \right] \right] . \quad (\text{B16})$$

The physical interpretation of the various terms in Eqs. (B14) is given in the text. The form of these equations can also be obtained from formulas given in Refs. 22 and 23, although we have derived them in a simpler form that is especially suited to the type of laser considered here.

\*Permanent address: Physics Department, Warsaw University, Warsaw, Poland.

<sup>1</sup>T. W. Hänsch, A. L. Schawlow, and P. E. Toschek, IEEE J. Quantum Electron. **QE-8**, 802 (1972).

<sup>2</sup>V. M. Baev, T. P. Belikova, É. A. Sviridenkov, and A. F. Suchkov Zh. Eksp. Teor. Fiz. **74**, 43 (1978) [Sov. Phys.—JETP **47**, 21 (1978)].

<sup>3</sup>F. T. Hioe, J. Math. Phys. **19**, 1307 (1978).

<sup>4</sup>V. M. Baev, T. P. Belikova, S. A. Kovalenko, É. A. Sviridenkov, and A. F. Suchkov Kvant. Elektron. (Moscow) **7**, 903 (1980) [Sov. J. Quantum Electron. **10**, 517 (1980)].

<sup>5</sup>V. R. Mironenko and V. I. Yudson, Opt. Commun. **34**, 397 (1980).

<sup>6</sup>V. M. Baev, G. Gaida, H. Schröder, and P. E. Toschek, Opt. Commun. **38**, 309 (1981).

<sup>7</sup>S. A. Kovalenko, Kvant. Elektron. (Moscow) **8**, 1271 (1981) [Sov. J. Quantum Electron. **11**, 759 (1981)].

<sup>8</sup>W. Brunner and H. Paul, Opt. Quant. Electron. **14**, 453 (1982).

<sup>9</sup>V. R. Mironenko and V. I. Yudson, Opt. Commun. **41**, 126 (1982).

<sup>10</sup>L. A. Westling, M. G. Raymer, M. G. Sceats, and D. F. Coker, Opt. Commun. **47**, 212 (1983).

<sup>11</sup>E. N. Antonov, A. A. Kachanov, V. R. Mironenko, and T. V. Plakhotnik, Opt. Commun. **46**, 126 (1983).

<sup>12</sup>W. Brunner, R. Fischer, and H. Paul, J. Opt. Soc. Am. B **2**, 202 (1985).

<sup>13</sup>H. Atmanspacher, H. Scheingraber, and C. R. Vidal, Phys. Rev. A **32**, 254 (1985).

<sup>14</sup>H. Atmanspacher, H. Scheingraber, and C. R. Vidal, Phys. Rev. A **33**, 1052 (1986).

<sup>15</sup>H. Atmanspacher and H. Scheingraber, Phys. Rev. A **34**, 253 (1986).

<sup>16</sup>H. Atmanspacher, H. Scheingraber, and V. M. Baev, Phys. Rev. A **35**, 142 (1987).

<sup>17</sup>Yu. M. Alvazyan, V. M. Baev, V. V. Ivanov, S. A. Kovalenko, and É. A. Sviridenkov, Kvant. Elektron. (Moscow) **14**, 279 (1987) [Sov. J. Quantum Electron. **17**, 168 (1987)].

<sup>18</sup>L. Pakhomycheva, E. Sviridenkov, A. Suchkov, L. Titova, and S. Churilov, Pis'ma Zh. Eksp. Teor. Fiz. **12**, 60 (1970) [JETP Lett. **12**, 43 (1970)].

<sup>19</sup>For a review, see S. J. Harris, Appl. Opt. **23**, 1311 (1984).

<sup>20</sup>T. P. Belikova, É. A. Sviridenkov, and A. F. Suchkov, Opt. Spectrosc. **37**, 372 (1974).

<sup>21</sup>P. Lett and L. Mandel, J. Opt. Soc. Am. B **2**, 1615 (1985).

<sup>22</sup>M. Sargent III, M. O. Scully, and W. E. Lamb, Jr., *Laser*

*Physics* (Addison-Wesley, Reading, MA, 1974).

<sup>23</sup>H. Haken, *Light, Vol. 2, Laser Light Dynamics* (North-Holland, Amsterdam, 1985).

<sup>24</sup>H. Risken and K. Nummedal, J. Appl. Phys. **39**, 4662 (1968).

<sup>25</sup>R. Graham and H. Haken, Z. Phys. **213**, 420 (1968).

<sup>26</sup>L. A. Kotomtseva, N. A. Loiko, and A. M. Samson, J. Opt. Soc. Am. B **2**, 232 (1985).

<sup>27</sup>L. A. Lugiato, L. M. Narducci, E. V. Eschenazi, D. K. Bandy, and N. B. Abraham, Phys. Rev. A **32**, 1563 (1985).

<sup>28</sup>L. M. Narducci, J. R. Tredicce, L. A. Lugiato, N. B. Abraham, and D. K. Bandy, Phys. Rev. A **33**, 1842 (1986).

<sup>29</sup>M. G. Raymer, I. McMackin, C. Radzewicz, M. Beck, and Z. Deng, Technical Digest, International Workshop on Instabilities, Dynamics and Chaos in Nonlinear Optical Systems, Il Ciocco, Lucca, Italy, 1987 (unpublished).

<sup>30</sup>C. L. Tang, H. Statz, and G. deMars, J. Appl. Phys. **34**, 2289 (1963).

<sup>31</sup>C. T. Pike, Opt. Commun. **10**, 14 (1974).

<sup>32</sup>I. V. Hertel and A. S. Stamatović, IEEE J. Quantum Electron. **QE-11**, 210 (1975).

<sup>33</sup>Manufactured by Victor Kyburz AG, Safnern, Switzerland.

<sup>34</sup>H. Hürri, S. Leutwyler, and E. Schumacher, Rev. Sci. Instrum. **53**, 1855 (1982).

<sup>35</sup>I. McMackin, C. Radzewicz, and M. G. Raymer J. Opt. Soc. Am. B **4**, 86 (1987).

<sup>36</sup>D. J. Gauthier, P. Narum, and R. W. Boyd, Opt. Lett. **11**, 623 (1986).

<sup>37</sup>P. Grassberger and I. Procaccia, Physica **9D**, 189 (1983).

<sup>38</sup>H. G. Schuster, *Deterministic Chaos an Introduction* (Physik-Verlag, Weinheim, 1984).

<sup>39</sup>T. H. Chyba, E. C. Gage, R. Ghosh, P. Lett., L. Mandel, and I. McMackin, Opt. Lett. **12**, 422 (1987).

<sup>40</sup>J. D. Farmer, E. Ott, and J. A. Yorke, Physica **7D**, 153 (1983).

<sup>41</sup>P. Grassberger and I. Procaccia, Phys. Rev. A **28**, 2591 (1983).

<sup>42</sup>H. Haken, Phys. Lett. **53A**, 77 (1975).

<sup>43</sup>L. W. Casperson, J. Opt. Soc. Am. B **2**, 62 (1985).

<sup>44</sup>N. B. Abraham, L. A. Lugiato, P. Mandel, L. M. Narducci, and D. K. Bandy, J. Opt. Soc. Am. B **2**, 35 (1985).

<sup>45</sup>L. Hillman, J. Krasinski, R. W. Boyd, and C. R. Stroud, Jr., Phys. Rev. Lett. **52**, 1605 (1984).

<sup>46</sup>L. Hillman, J. Krasinski, K. Koch, and C. R. Stroud, Jr., J. Opt. Soc. Am. B **2**, 211 (1985).

<sup>47</sup>The derivation leading to Eqs. (B6) is due to P. W. Milonni (private communication).

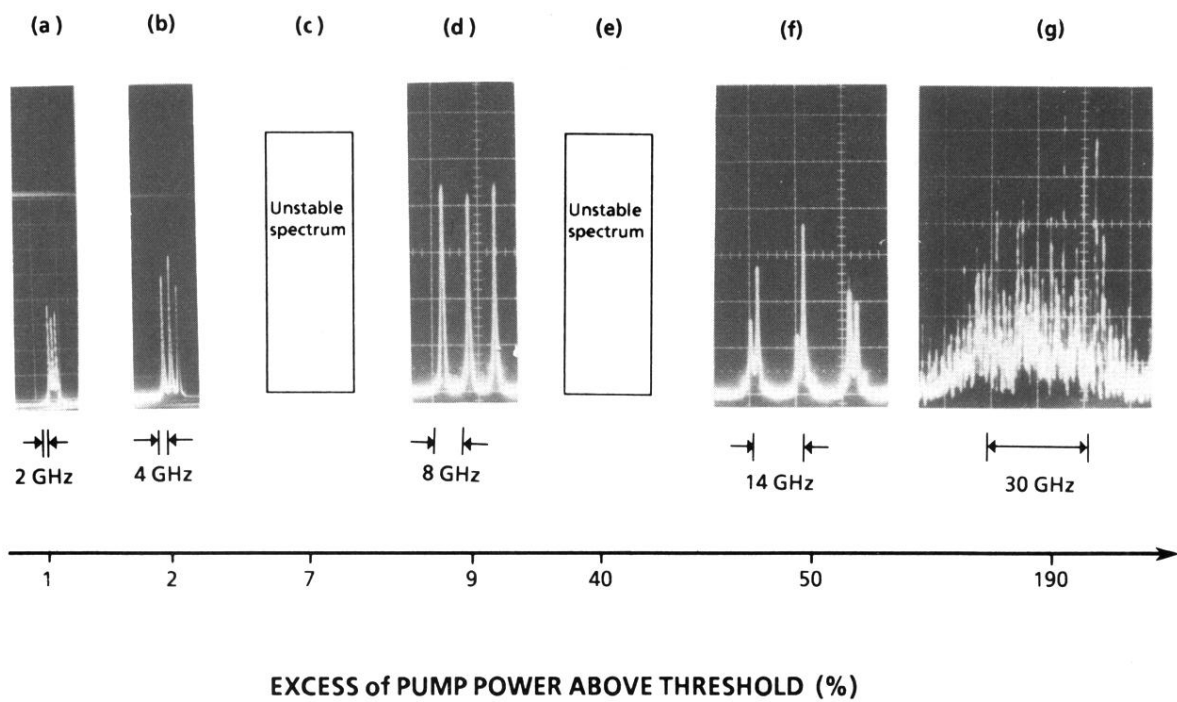


FIG. 2. Dye-laser optical spectrum as a function of excess of pump power above threshold.